Generic functional modelling of multi-pulse auto-transformer rectifier units for more-electric aircraft applications

Tao YANG [a],*, Serhiy BOZHKO [a], Patrick WHEELER [a], Shaoping WANG [b], Shuai WU [b]

[a] *Department of Electrical and Electronic Engineering, University of Nottingham, Nottingham NG72RD, UK*
[b] *School of Automation Science and Electrical Engineering, Beihang University, Beijing 100083, China*

Abstract   The Auto-Transformer Rectifier Unit (ATRU) is one preferred solution for high-power AC/DC power conversion in aircraft. This is mainly due to its simple structure, high reliability and reduced kVA ratings. Indeed, the ATRU has become a preferred AC/DC solution to supply power to the electric environment control system on-board future aircraft. In this paper, a general modelling method for ATRUs is introduced. The developed model is based on the fact that the DC voltage and current are strongly related to the voltage and current vectors at the AC terminals of ATRUs. In this paper, we carry on our research in modelling symmetric 18-pulse ATRUs and develop a generic modelling technique. The developed generic model can study not only symmetric but also asymmetric ATRUs. An 18-pulse asymmetric ATRU is used to demonstrate the accuracy and efficiency of the developed model by comparing with corresponding detailed switching SABER models provided by our industrial partner. The functional models also allow accelerated and accurate simulations and thus enable whole-scale more-electric aircraft electrical power system studies in the future.

© 2018 Production and hosting by Elsevier Ltd. on behalf of Chinese Society of Aeronautics and Astronautics. This is an open access article under the CC BY-NC-ND license (http://creativecommons.org/licenses/by-nc-nd/4.0/).

1. Introduction

Driven by the demand to optimize aircraft performance, decrease operation and maintenance costs and reduce noise pollution, the aircraft industry has been pushed towards the concept of the More-Electric Aircraft (MEA). In the MEA, many functions which are conventionally managed by hydraulic, pneumatic and mechanical power, will be replaced with devices driven by electrical power.[1,2] Such replacement would

reduce system weight and volume, increase overall reliability, capability and maintainability, and provide higher durability for aircraft operations.[3] Aircraft power electronics have also been affected by this trend. The need for power conversion and driving equipment on-board has become significant. Recently, the usage of AC-DC conversion has become a common feature for aircraft power distribution systems. In general, there are two main types of this AC-DC power conversion: the PWM active front-ends and passive multi-phase transformer rectifiers. The former has seen increased application incorporation such as electromagnetic actuators[4] and electrical starter-generator applications.[5] However, the latter seems to be the main power source for high-power DC load such as aircraft Environment Control Systems (ECS) due to its simple structure and high reliability. The civil aircraft has long been using Transformer Rectifier Unit (TRU) to produce 28 VDC from 115 V, 400 Hz ACsources. However, recently the auto-transformer rectifier has received more attention in aerospace industry due to its reduced kVA rating compared with TRUs.[6]

A number of possible ATRU topologies have been proposed during the last decade.[7–13] These ATRUs can be categorized into 12-pulse types, 18-pulse types, 24-pulse types, etc., according to the number of pulses in the rectified voltage or in the line current during one fundamental cycle. Among these topologies, the 18-pulse ATRU seems to be a preferable option. This is due to the fact that it has higher power quality than the 12-pulse type and less devices than the 24-pulse or other higher pulse type ATRUs. The 18-pulse ATRU is now actually being used on-board B787, the Dreamliner, supplying power to the environment control system.[14]

The 18-pulse ATRUs can be divided into symmetric and asymmetric types depending on the symmetry of voltages on the secondary side of the transformer. For symmetric 18-pulse ATRUs, the voltages on the secondary side of the auto-transformer are with the same magnitude (normally the same with the magnitude of voltage on the primary side) and have an equal phase shift of 40° from each other. The load power is equally shared by the three directly-connected diode bridges. For asymmetric 18-pulse ATRUs, however, the voltages on the secondary side are of different magnitudes. The voltage phase-shift angle is also not necessarily 40°.

The increased power electronics and motor drives on-board MEA are bringing significant modelling challenges due to its wide variation in time constant. The challenge is to balance the simulation speed against the model accuracy and this is dependent on the modelling task. Four different modelling layers are defined according to the modelling bandwidth, i.e. architectural models, functional models, behavioural models and component models[15,16] as shown in Fig. 1.

The architectural layer computes steady-state power flow and is used for weight, cost and cabling studies. In the functional level, the system components are modelled to handle the main system dynamics up to 150 Hz. The error of models in this level should be less than 5% in respect of the behavioural model accuracy. The behavioural model uses lumped-parameter subsystem models and the modelling frequencies can be up to hundreds of kHz. The component models cover high frequencies, electromagnetic field and ElectroMagnetic Compatibility (EMC) behaviour, and perhaps thermal and mechanical stressing. The bandwidth of component models can be up to MHz region if required.[16]
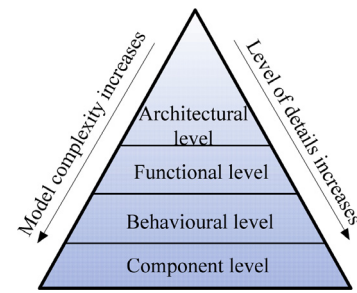

Fig. 1   Multi-level modelling paradigm.[16]

This paper aims to develop a general functional model of ATRUs which allows future engineers to study ATRUs in a more efficient and effective way. The functional models allow accelerated and accurate simulations and thus enable a whole-scale MEA Electrical Power System (EPS) studies in the future. The developed ATRU model is based on the vector concept and in the synchronous dq frame. This method has been widely used in modelling electrical machines.[16–18]

The remainder of the paper is organized as follows: Section 2 briefly outlines the operation of ATRUs; Section 3 gives details of the development of the proposed modelling technique; an 18-pule ATRU is used for the effectiveness and efficiency studies in Section 4; Section 5 draws the conclusions of the paper.

2. Operation principles

The design of multiphase transformer rectifiers has been well discussed in Ref. [19]. The auto-transformer rectifiers normally comprise a phase-shift transformer and a set of three-phase diode bridges as shown in Fig. 2. The phase shift transformer is not necessarily an auto-transformer type. However, the auto-transformer is a preferred option due to its low kVA ratings. In this paper, we mainly focus on auto-transformer rectifier units.

As can be observed in Fig. 2, the auto-transformer is used to create three sets of three-phase voltages on the secondary side, i.e. (v_{a1}, v_{b1}, v_{c1}), (v_{a2}, v_{b2}, v_{c2}) and (v_{a3}, v_{b3}, v_{c3}). These resultant 9 phases are then fed into three diode bridges supplying power to the dc link. At each instant of time, there are two diodes conducting. These two conducting diodes allow the largest line-to-line voltage to be applied to the DC side. We refer to the ATRU system shown in Fig. 2 as a "3-9-DC" system. For some ATRUs, especially asymmetric ones, the voltage sources on the primary side of the transformer also feed
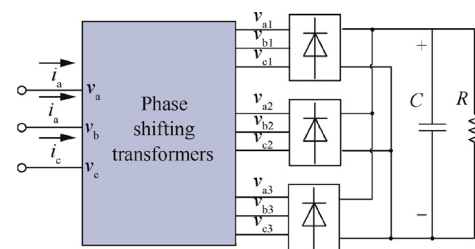

Fig. 2   General auto-transformer rectifier units.

directly into one diode bridge, i.e. one diode bridge is directly connected to the primary side. In this paper, we consider that the voltage set (v_{a1}, v_{b1}, v_{c1}) is the same as that from the primary side, i.e. (v_a, v_b, v_c).

3. General functional model of 18-pulse ATRUs

A general functional modelling method for the 18-pulse ATRUs will be detailed in this section. Although the development process is similar to our previous work for a symmetric 18-pulse ATRU in Ref. [20], this paper extends this modelling technique to more general ATRU topologies and thus covers both symmetric and asymmetric ATRUs. However, the basic concept of model development keeps the same. In summary, development of the functional model will involve the following four steps:

Step 1. Reducing the 3-9-DC system in Fig. 2 into a 3-3-DC system as shown in Fig. 3, where R_{eq} and L_{eq} are the equivalent resistance and inductance of the autotransformer. This can be achieved using auto-transformer voltage and current relations between primary and the selected channel on the secondary side (marked as v_{as}, v_{bs} and v_{cs} in Fig. 3).
Step 2. Transforming the 3-3-DC system into the dq frame.
Step 3. Using the space vector concept to derive the relationship between the chosen channel voltage and current vectors (v_s and i_s) and the rectified voltage and current v_{dc} and i_{dc}.
Step 4. Identifying the equivalent leakage inductance and resistance.

The reduced-order ATRU model is divided into three parts as shown in Fig. 3: An ideal transformer, an equivalent RL circuit and an AC/DC converter. The development of functional models for each part will be detailed in the following sections.

3.1. Ideal transformer

For any transformer or auto-transformer, the voltages on the primary side and the secondary side are strongly coupled. Some typical auto-transformers for 18-pulse ATRUs are shown in Fig. 4.

Fig. 4(a) and (b) show three types of auto-transformer for symmetrical ATRUs and their associated voltage phasor diagrams. It can be seen that the voltage phasors on the primary side (V_a, V_b, V_c) and the secondary side (V_{a1}, V_{b1}, V_{c1}), (V_{a2}, V_{b2}, V_{c2}) and (V_{a3}, V_{b3}, V_{c3}) are of the same magnitude. The

primary voltages also supply one set of diode bridges directly. The voltage phasors divide the plane equally with 40° phase shift from each other. When these transformers are used for 18-pulse ATRU applications, the primary voltage source, together with the secondary windings, is used to feed the three sets of diode bridges. The auto-transformer shown in Fig. 4(c) is an asymmetric auto-transformer where the voltages of the primary and secondary side are of different magnitudes. The phase shift between primary and secondary sides is 37° instead.

The corresponding phase diagram in Fig. 4 can be given in Fig. 5.

From the phasor diagrams in Fig. 5, we can derive that the corresponding three-phase voltages on secondary sides (v_{a2}, v_{b2}, v_{c2}) can be given as a function of three-phase voltages (v_a, v_b, v_c) on the primary side. One set of the three-phase voltages on the secondary side of the transformer (take v_{a2}, v_{b2} and v_{c2} as examples) can be given in a general form irrelevant to the auto-transformer types as

$$
\begin{cases}
v_{a2} = v_a + \frac{k_1}{\sqrt{3}}(v_b - v_c) + \frac{k_2}{\sqrt{3}}(v_b - v_a) \\
v_{b2} = v_b + \frac{k_1}{\sqrt{3}}(v_c - v_a) + \frac{k_2}{\sqrt{3}}(v_c - v_b) \\
v_{c2} = v_c + \frac{k_1}{\sqrt{3}}(v_a - v_b) + \frac{k_2}{\sqrt{3}}(v_a - v_c)
\end{cases}
\tag{1}
$$

where k_1 and k_2 are the turn ratios between the primary and secondary windings of the transformer. For the configurations in Fig. 5, the turn ratio k_1 and k_2 are given as

These parameters can be calculated from the phasor diagram in Fig. 5 with designed secondary voltage magnitudes and shift angles. Eq. (1) can be written in matrix form as

$$
\begin{bmatrix} v_{a2} \\ v_{b2} \\ v_{c2} \end{bmatrix} =
\begin{bmatrix}
1 - \frac{k_2}{\sqrt{3}} & \frac{k_1}{\sqrt{3}} + \frac{k_2}{\sqrt{3}} & -\frac{k_1}{\sqrt{3}} \\
-\frac{k_1}{\sqrt{3}} & 1 - \frac{k_2}{\sqrt{3}} & \frac{k_1}{\sqrt{3}} + \frac{k_2}{\sqrt{3}} \\
\frac{k_1}{\sqrt{3}} + \frac{k_2}{\sqrt{3}} & -\frac{k_1}{\sqrt{3}} & 1 - \frac{k_2}{\sqrt{3}}
\end{bmatrix}
\begin{bmatrix} v_a \\ v_b \\ v_c \end{bmatrix} = A \begin{bmatrix} v_a \\ v_b \\ v_c \end{bmatrix}
\tag{2}
$$

where the matrix A is defined as

$$
A = \begin{bmatrix}
1 - \frac{k_2}{\sqrt{3}} & \frac{k_1}{\sqrt{3}} + \frac{k_2}{\sqrt{3}} & -\frac{k_1}{\sqrt{3}} \\
-\frac{k_1}{\sqrt{3}} & 1 - \frac{k_2}{\sqrt{3}} & \frac{k_1}{\sqrt{3}} + \frac{k_2}{\sqrt{3}} \\
\frac{k_1}{\sqrt{3}} + \frac{k_2}{\sqrt{3}} & -\frac{k_1}{\sqrt{3}} & 1 - \frac{k_2}{\sqrt{3}}
\end{bmatrix}
\tag{3}
$$

Assuming that all the power is transferred through the transformer from the chosen channel in order to reduce the system order, we can derive

$$
\begin{bmatrix} i_a \\ i_b \\ i_c \end{bmatrix}^T
\begin{bmatrix} v_a \\ v_b \\ v_c \end{bmatrix} = k_p
\begin{bmatrix} i_{a2} \\ i_{b2} \\ i_{c2} \end{bmatrix}^T
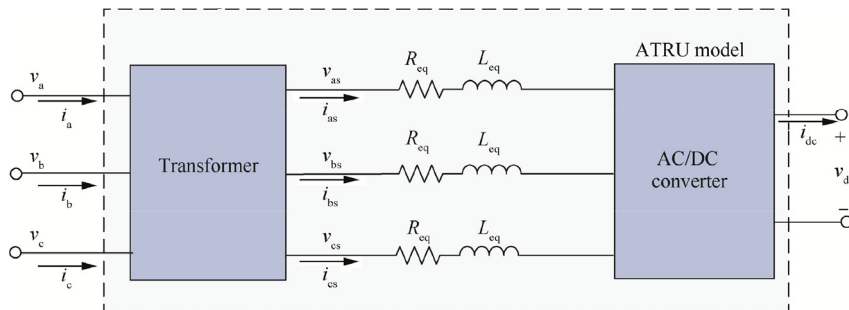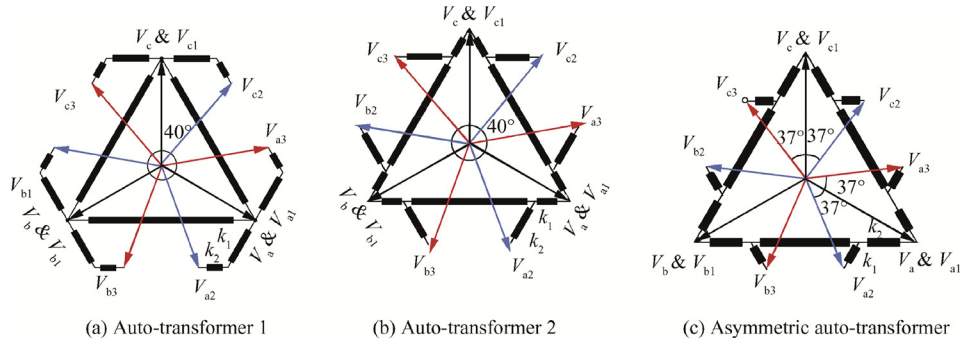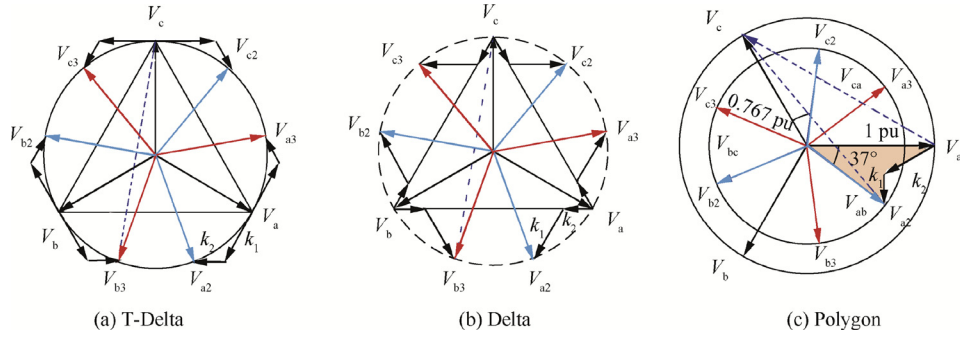\begin{bmatrix} v_{a2} \\ v_{b2} \\ v_{c2} \end{bmatrix}
\tag{4}
$$

Fig. 3 Equivalent representation of ATRU.

Fig. 4   T-Delta and Delta winding configurations of different types of 18-pulse ATRU.[21]

Fig. 5   Phasor diagram of symmetric T-Delta type, Delta, Polygon winding for symmetric ATRU and asymmetric D-ATRU.

where k_p is called the power balance coefficient. This coefficient is to ensure that the power is balanced between primary and secondary sides of the transformer. This coefficient k_p is exclusively dependant on the configuration of the transformer. The calculation of k_p will be explained in Section 3.2.4. Substituting Eq. (2) into Eq. (4) yields

$$\begin{bmatrix} i_a \\ i_b \\ i_c \end{bmatrix} = k_p \boldsymbol{A}^T \begin{bmatrix} i_{a2} \\ i_{b2} \\ i_{c2} \end{bmatrix} \quad (5)$$

The transformation from the abc three-phase coordination to the dq frame is considered as

$$f_{dq} = \boldsymbol{K}_s f_{abc} \quad (6)$$

where f_{abc} represents variables in the three-phase coordinate;

$$\boldsymbol{K}_s = \frac{2}{3} \begin{bmatrix} \cos\theta & \cos(\theta - 2/3\pi) & \cos(\theta + 2/3\pi) \\ -\sin\theta & -\sin(\theta - 2/3\pi) & -\sin(\theta + 2/3\pi) \end{bmatrix} \quad (7)$$

where θ is the synchronous angle and $\theta = \int \omega dt$, ω is the angular speed of the rotating dq frame Transforming Eqs. (2) and (5) by multiplying both sides by Eq. (7) yields

$$\begin{bmatrix} v_{d2} \\ v_{q2} \end{bmatrix} = \begin{bmatrix} 1 - \sqrt{3}k_2/2 & k_1 + 0.5k_2 \\ -(k_1 + 0.5k_2) & 1 - \sqrt{3}k_2/2 \end{bmatrix} \begin{bmatrix} v_d \\ v_q \end{bmatrix} \quad (8)$$

$$\begin{bmatrix} i_d \\ i_q \end{bmatrix} = k_p \begin{bmatrix} 1 - \sqrt{3}k_2/2 & -(k_1 + 0.5k_2)_2 \\ k_1 + 0.5k_2 & 1 - \sqrt{3}k_2/2 \end{bmatrix} \begin{bmatrix} i_{d2} \\ i_{q2} \end{bmatrix} \quad (9)$$

Eqs. (8) and (9) establish the relationship between the voltages and currents of the primary winding and the selected secondary winding of an auto-transformer. The dq transformation, essentially, is to project the voltage and current vectors into a synchronous reference frame. The vector is defined as

$$\boldsymbol{x} = \frac{2}{3}(x_a + x_b e^{j2\pi/3} + x_c e^{j4\pi/3}) \quad x = v, i \quad (10)$$

The magnitude of voltage or current vectors in Eq. (10) is equal to its corresponding peak phase value. The relation of vector magnitudes between the primary and secondary sides (the second channel) of the transformer is give as

$$\|\boldsymbol{v}_2\| = k_v \|\boldsymbol{v}\| \quad (11)$$

$$\|\boldsymbol{i}\| = k_v k_p \|\boldsymbol{i}_2\| \quad (12)$$

where $\|\cdot\|$ is the magnitude of the corresponding vector, and k_v is the ratio between the magnitude of voltages on primary and secondary sides of the transformer. The magnitudes of vectors can be calculated in the dq frame as

$$\|\boldsymbol{x}\| = \hat{x} = \sqrt{x_d^2 + x_q^2} \quad (13)$$

where $\boldsymbol{x}$ can be voltage or current, and $\hat{x}$ is the peak value of $\boldsymbol{x}$.

3.2. AC-DC converter

With the vector concept introduced in Section 3.1 the voltage and current relations for the AC-DC converter parts shown in Fig. 3 will be detailed in this section.

3.2.1. Voltage

For any multi-phase rectifier, the dc-link voltage is always equal to the maximum line-to-line voltage on the AC side at any instant of time. In a phasor diagram, the line-to-line voltage phasors implemented on the DC side of diode bridges are essentially those with the largest distance between two phase voltages as shown in bold dotted lines in Fig. 5. For an 18-pulse ATRU, these line-to-line voltage phasors always operate for $\pi/9$ period as shown in Fig. 6. In addition, each phasor and its opposite phasor (V_{cb1} and V_{b1c} for example) are with the same terminals but connected to dc-link capacitor in opposite.

It can also be noticed that for symmetric ATRUs, each diode carries $2\pi/9$ period of i_{dc}. For example, during the period with phasors from V_{c2b1} to V_{cb1} then V_{ca2}, the lower diode at phase b1 conducts for $\pi/9$ when V_{c2b1} is active and another $\pi/9$ when V_{cb1} is active as shown in Fig. 6(a).

For the asymmetric, however, the terminals (a1, b1, c1) & (a2, b2, c2) on the secondary side conduct for only $\pi/9$ as shown in Fig. 6(b).

For example, from V_{ac} to V_{ac2} and then V_{ab1}, the terminal c2 only conducts for $\pi/9$ period.

(a) Delta-type symmetric ATRU   (b) Delta-type asymmetric ATRU
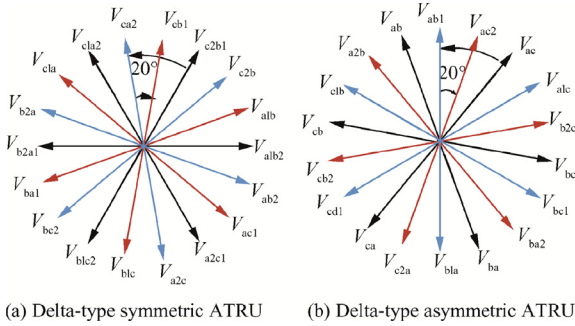
Fig. 6 Line-to-line voltage phasor reflected on DC-link side of ATRU.
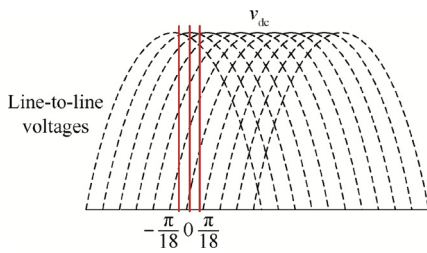
Fig. 7 Relations between line-to-line voltages and DC-link voltage.

Considering that the line-to-line voltage phasors are of the same magnitude and each of them functions for $\pi/9$ period, the relation between the dc-link voltage and line-to-line voltages is shown in Fig. 7.

With Fig. 7, we can derive that the dc-link voltage v_{dc} is the average value of a line-to-line voltage around its peak for a period $[-\pi/18, \pi/18]$ and can be given as

$$v_{dc} = \frac{9}{\pi} \int_{-\pi/18}^{\pi/18} \hat{V}_{ll} \cos\theta \, d\theta \tag{14}$$

where $\hat{V}_{ll}$ is the magnitude of line-to-line voltages in Fig. 6 and can be calculated from phase peak voltage value $\hat{V}_{\alpha}$. With Eq. (14), we have the following table.

In Table 1, $\hat{V}_a$ is the maximum value of the phase voltage v_a and is equal to the magnitude of v, denoted as $\|v\|$, and $\hat{V}_{a2}$ is the maximum value of the phase voltage v_{a2} and is equal to the magnitude of v_{a2}.

3.2.2. Current

As mentioned before, the conduction period of each phase at the secondary side of the ATRUs is dependent on the topology of the transformers. If we only consider the fundamentals of the currents at the AC side of the diode bridges, the relationship between i_2 and i_{dc} can be written as

$$\|i_2\| = \frac{4\sin\varphi}{\pi} i_{dc} \tag{15}$$

The angle ϕ is half of the conduction period of diodes connected to the selected channel. For asymmetric ones, ϕ is $\pi/9$. For asymmetric ones shown in Fig. 4, ϕ is equal to $\pi/18$. If we neglect the internal inductance, the snubber resistance, and the capacitance of the diodes and assume there is no energy storage within a diode rectifier, the fundamental components of voltage and current on the AC side are in phase. Thus the phase angle of the AC current vector can be given from the voltage vector as

$$\theta_{i_2} = \arctan(v_{q2}/v_{d2}) \tag{16}$$

Hence, the currents on the d and q axes are

$$i_{d2} = \|i_2\| \cos\theta_{i_2} \tag{17}$$

$$i_{q2} = \|i_2\| \sin\theta_{i_2} \tag{18}$$

3.2.3. Commutation loss

Analysis of commutation loss for an 18-pulse rectifier can begin from the study of a 6-pulse diode rectifier. Considering that the commutation occurs every $\pi/9$, the voltage drop thus can be expressed as

Table 1 Relations between DC-link voltage v_{dc} and voltage vectors of auto-transformers.

Item	Symmetric Delta-type ATRUs	Asymmetric Delta-type ATRUs
Maximum line-to-line voltage $\hat{V}_{ll}$	$\hat{V}_{ll} = \hat{V}_{cb1} = 2\hat{V}_a \cos(\pi/18)$	$\hat{V}_{ll} = \hat{V}_{ab} = \sqrt{3}\hat{V}_a$
Relation between DC-link voltage v_{dc} and phase peak voltage $\hat{V}_a$	$v_{dc} = \frac{18}{\pi}\hat{V}_a \sin(\pi/9)$	$v_{dc} = \sqrt{3}\hat{V}_a \frac{\sin(\pi/18)}{\pi/18}$
Relation between DC-link voltage v_{dc} and voltage vector v_2 dq components*	$v_{dc} = \frac{\sqrt{v_{d2}^2 + v_{q2}^2}}{k_v} \frac{\sin(\pi/9)}{\pi/18}$	$v_{dc} = \frac{\sqrt{v_{d2}^2 + v_{q2}^2}}{k_v} \frac{\sqrt{3}\sin(\pi/18)}{\pi/18}$

* This row considers the relation between $\hat{V}_a$ and $\hat{V}_{a2}$ as illustrated in Eq. (11).

$$\Delta V_\mathrm{d} = \frac{\omega L_\mathrm{s} i_\mathrm{dc}}{\pi/9} = \frac{9}{\pi} \omega L_\mathrm{s} i_\mathrm{dc} \tag{19}$$

Combining dc-link voltage in Table 2 and Eq. (19), the DC link voltage can be written as

$$v_\mathrm{dc} = \sqrt{3} \hat{V}_\mathrm{a} \frac{\sin(\pi/18)}{\pi/18} - \frac{9}{\pi} \omega L_\mathrm{s} i_\mathrm{dc} \tag{20}$$

3.2.4. Calculation of k_p

The power balance coefficient k_p is derived using the principle of power balance between the AC and DC sides of the ATRU. This has been detailed discussed in Ref. [20] and will be briefly introduced in this section.

The power on the DC side can be calculated as

$$P_\mathrm{dc} = v_\mathrm{dc} i_\mathrm{dc} = \sqrt{3} \frac{\sin(\pi/18)}{\pi/18} \hat{V}_\mathrm{a} i_\mathrm{dc} \tag{21}$$

Assuming that there is no provision for energy storage and power losses in the diode bridge, the fundamental component of current at the input must be in phase with the input voltage (as the output current is in phase with the output voltage).[19] The power at the AC side can be expressed as

$$P_\mathrm{ac} = \frac{3}{2} \|\boldsymbol{v}\| \|\boldsymbol{i}\| = \frac{3}{2} k_\mathrm{v} k_\mathrm{p} \frac{4 \sin(\pi/18)}{\pi} \hat{V}_\mathrm{a} i_\mathrm{dc} \tag{22}$$

Using power balance $P_\mathrm{dc} = P_\mathrm{ac}$ and combining Eqs. (21) and (22), we can derive

$$k_\mathrm{p} = \frac{3\sqrt{3}}{k_\mathrm{v}} \tag{23}$$

3.3. Equivalent RL circuit

The parameters L_eq and R_eq are given as

$$L_\mathrm{eq} = L_\mathrm{s} + \frac{L_\mathrm{p}}{N^2} \tag{24}$$
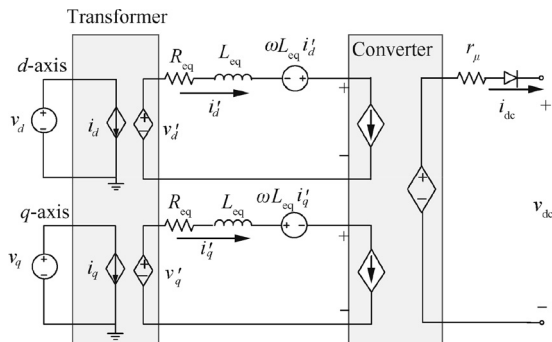
$$R_\mathrm{eq} = R_\mathrm{s} + \frac{R_\mathrm{p}}{N^2} \tag{25}$$

where L_p and L_s are the primary and secondary leakage inductances respectively, R_p and R_s are the primary and secondary winding resistances respectively, and N is the turn ratio between the primary and secondary windings.

Summarizing this section, the developed DQ model of the overall asymmetrical ATRU can be presented by Fig. 8. As can be seen, the model includes three parts, i.e. the transformer, RL circuits and the converter. The auto-transformer and converter are represented as controlled current and voltage sources. The developed DQ model can be interfaced with other models developed in the dq frame as in Ref. [16,22], where ideal three-phase sources, synchronous machines, transmission lines, etc. are introduced. A three-phase voltage source will become two DC sources in the dq-frame model, as shown in Fig. 8. The developed DQ model can connect with models developed in the three-phase coordinate frame, by using a three-phase to dq frame interface. The developed model can be used for both balanced and unbalanced conditions as discussed in Ref. [20]. The procedure of developing functional models of asymmetric ATRUs can be summarised by the flowchart in Fig. 9.

4. Simulation results of asymmetric example

The generic functional model has been successfully implemented to a D-type symmetric 18-pulse ATRU in our previous publication.[20] In this section, we will demonstrate the effectiveness of the technique in modelling a D-type asymmetric ATRU. This asymmetric ATRU, shown in Fig. 4, will be tested and validated by comparison to a corresponding behavioural model under both balanced and unbalanced conditions. The original behavioural model of the ATRU was developed in SABER provided by our industrial partner and has been validated before release. The behavioural model (ABC model) considers the leakage inductance of the transformer as well as the switching behaviour of the diodes in the converter. The simulation scheme is shown in Fig. 10. Simulations have been performed on an Intel i7 CPU@3.20 GHz,

Table 2   Turn ratios for different auto-transformers.

Auto-transformer types	Values of k_1 and k_2
T type in Fig. 4(a)	$k_1 = 0.51, k_2 = 0.27$
D type in Fig. 4(b)	$k_1 = 0.51, k_2 = 0.27$
D type in Fig. 4(c)	$k_1 = 0.45, k_2 = 0.24$

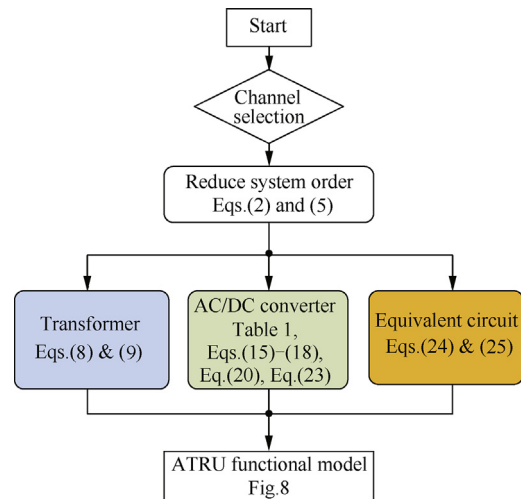**Fig. 8**   18-pulse asymmetric ATRU model in dq frame.

Fig. 9   Flowchart for development of ATRU DQ models.

24.0 GB of RAM using Dymola/Modelica v.7.4 software. The behavioural model is redeveloped in the Dymola from the original SABER model to enable the computation time studies comparing the behavioural model and the functional model. The Radau IIa algorithm has been chosen in the solver and the tolerance has been set at 1×10^{-4}. As a quantitative evaluation of the computational efficiency of these modelling techniques, the computation time has been compared. Meanwhile, the evaluation of the accuracy is performed by comparing the plots of the system quantities.

4.1. Line-to-ground fault

In this section, the developed DQ model is simulated and tested under line-to-ground fault conditions. The simulation scheme is shown in Fig. 10. The ATRU is supplied by an ideal three-phase voltage source with phase voltage $V_s = 230\text{VRMS}@400$ Hz. The transmission line is modelled as an RL circuit with $R_T = 0.1\ \Omega$ and $L_T = 1\ \mu\text{H}$. The DC-link capacitance $C = 260$ mF and the load resistance is set at 10 Ω. A line-to-ground fault is applied between phase A and the ground at the front end of the ATRU and the fault resistance R_{fault} is set at 100 $\mu\Omega$. Simulation results from the ABC model and the DQ model are compared in Fig. 11 and Fig. 12. From Fig. 11, it can be seen that under balanced conditions, the DC-link voltage v_{dc} in the ABC model includes high switching harmonics, while v_{dc} from the DQ model is with a constant value. Under line-to-ground fault conditions, a second harmonic (800 Hz) appears in the DC-link voltage of both the ABC and DQ models. This is mainly due to the fact that with an unbalanced power supply, the multi-pulse rectifier is reduced to a single-phase diode rectifier. In the DQ model, the second harmonic appears in both d and q axes. The results from the two models are very well matched under both balanced and unbalanced conditions. The AC currents flowing into the ATRU are shown in Fig. 11. The currents from the ABC model and DQ model match very well under both balanced and line-to-ground fault conditions. After the line-to-ground fault occurs at 0.1 s, since phase A is short-circuit to the ground, there is only a small leakage current, i_a, flowing through phase A.

4.2. Line-to-line fault

The developed model was also tested under line-to-line fault conditions. The system scheme is shown in Fig. 10 with a line-to-line fault between phase A and phase B at $t = 0.05$ s. The parameters keep the same as those used in Section 4.1.
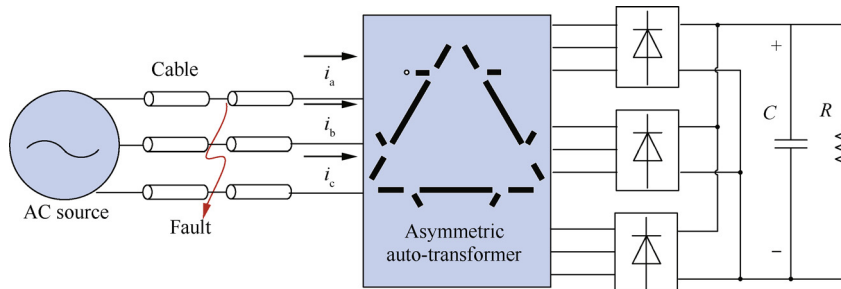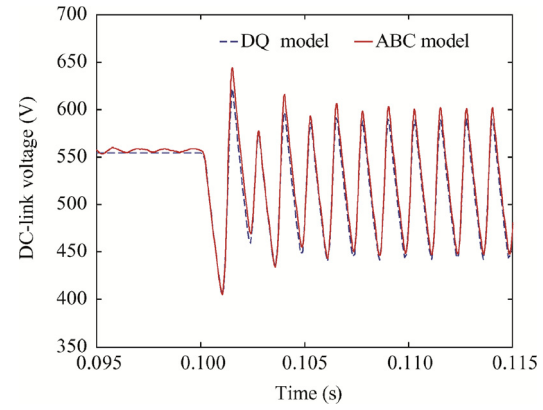

Fig. 11 DC-link voltage comparison between ABC model and DQ model with a line-to-ground fault occurring at $t = 0.1$ s.
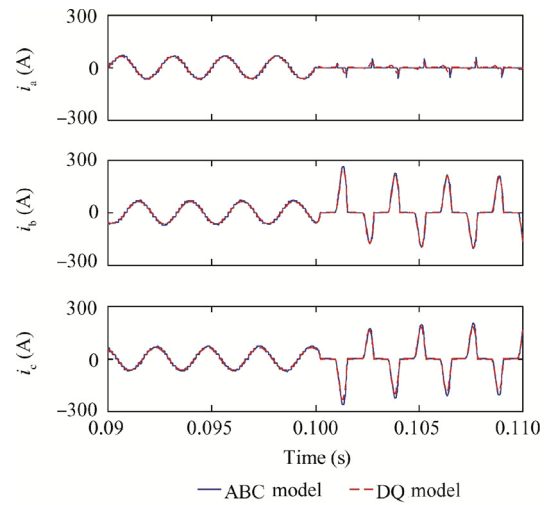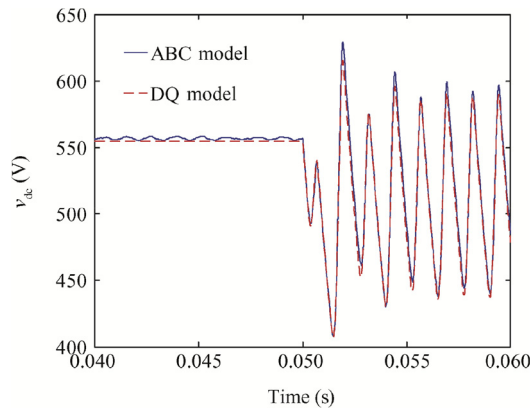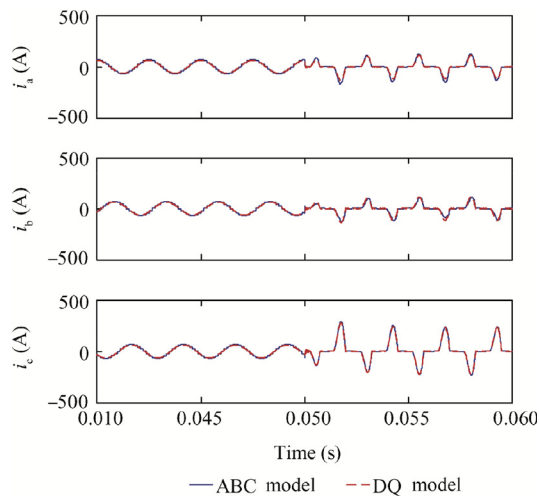

Fig. 12 Comparison of AC side currents within ABC model and DQ model with a line-to-ground fault occurring at $t = 0.1$ s.

The DC-link voltage at the output of the ATRU, and currents flowing into the ATRU, are shown in Figs. 13 and 14 respectively. As can be seen from these two figures, the results from the DQ model and the ABC model match very well under both balanced and line-to-line fault conditions. It is important to note that both models match very well after the fault occurs; phase A and phase B equally share the currents under line-to-line fault conditions and the sum of these two currents is equal to the current flowing in phase C i_c.

Fig. 10 Simulation scheme of ATRU under line fault conditions.

Fig. 13 DC-link voltage comparison between ABC model and DQ model with a line-to-line fault occurring at $t = 0.05$ s.


Fig. 14 Comparison of AC side currents within ABC model and DQ model with a line-to-line fault occurring at $t = 0.05$ s.

Table 3 CPU time comparison between ABC and DQ models.

Scenario	ABC	DQ	Acceleration
Before fault (0–0.05 s)	72.08	0.12	600
Total time (0–0.1 s)	**86.52**	5.081	17

Table 3 shows the computation time required by the two models under both balanced and unbalanced conditions. It can be seen that before the fault occurs, the DQ model is 600 times faster than the ABC model. This is because under balanced conditions, all the variables in the DQ model are DC-like. This allows the computer to use larger simulation steps. However, after the fault occurs, the simulation speed of DQ model decreases sharply. This is due to the second harmonics included in the DQ model under unbalanced conditions. Table 3 and Fig. 15 give a comparison of the CPU time required by the two models. Interestingly, Fig. 15 also shows that the simulation speed of the ABC model under
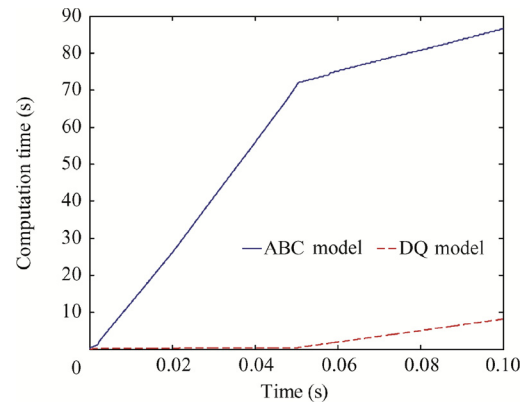
Fig. 15 CPU time comparison between ABC and DQ models with a step load change at $t = 0.02$ s and a line-to-line fault implemented at $t = 0.05$ s.

line-to-line fault conditions is faster than that under balanced conditions. This is due to the fact that with a line-to-line fault, or under unbalanced conditions, the number of conducting diodes in one period is reduced, i.e. less switching behaviour in one period.

5. Conclusions

In this paper, an averaging functional model framework based on the vector concept was introduced to study both symmetric and asymmetric ATRUs. The development of the functional model consisted of three steps: reducing the order of the system, transforming the reduced-order system into the DQ frame and defining the equivalent leakage inductance and resistance. The generic DQ model developed in this paper provides an accurate and computationally efficient method of modelling both symmetric and asymmetric ATRUs. In addition, the developed model can be conveniently connected to other functional DQ models developed from previous work. The interface between the DQ model and the ABC model can also be conveniently developed using a DQ/ABC transformation. Under balanced conditions, the DQ model is 600 times faster than ABC models. Under unbalanced conditions, the simulation speed of the DQ model decreases sharply. This is due to the double frequency in both d and q axes. The dynamic phasor technique is a potential method to handle an unbalanced system effectively. The dynamic phasor model for the 18-pulse ATRU is under development and will be published in future.

References

1. Quigley REJ. More electric aircraft. *Applied power electronics conference and exposition*; 1993. p. 906–11.
2. Sarlioglu B, Morris CT. More electric aircraft: review, challenges, and opportunities for commercial transport aircraft. *IEEE Trans Transport Electrific* 2015;**1**(1):54–64.

3. Uan-Zo-li A, Burgos R, Wang FD, Boroyevich F, Tardy A. Comparison of prospective topologies for aircraft autotransformer-rectifier units. *Conference of the IEEE industrial electronics society*; 2003 Nov 2–6; Roanoke. Piscataway:IEEE Press; 2003. p. 1122–7.

4. Wheeler P, Trentin A, Bozhko S, Clare J. Regeneration of energy onto an aircraft electrical power system from an electro-mechanical actuator. *Electrical systems for aircraft, railway and ship propulsion*; 2012 Octo 16-18; Bologna .2012. p. 1–6.

5. Bozhko S, Yeoh SS, Gao F, Hill C. Aircraft starter-generator system based on permanent-magnet machine fed by active front-end rectifier. *40th annual conference of the IEEE industrial electronics society*; 2014 Oct 29–Novrmber 1; Dallas. Piscataway:IEEE Press; 2014. p. 2958–64.

6. Choi S, Enjeti PN, Pitel IJ. Polyphase transformer arrangements with reduced kVA capacities for harmonic current reduction in rectifier-type utility interface. *IEEE Trans Power Electron* 1996;**11**(1):680–90.

7. Kamath GR, Benson D, Wood R. A novel autotransformer based 18-pulse rectifier circuit. *Applied power electronics conference and exposition*; 2002 Mar 10–14; Dallas. 2002. p. 795–801.

8. Paice DA. Nine-phase step-up/step-down autotransformer. United States Patent 7274280; 2007 September 25.

9. Burgos R, Uan-Zo-li A, Lacaux F, Wang F, Boroyevich D. Analysis and experimental evaluation of symmetric and asymmetric 18-pulse autotransformer rectifier topologies. *Power conversion conference*; 2007 Apr 2–5; Nagoya. 2007. p. 1286–93.

10. Wu X, Cai P, Zhang X. Design and analysis of an autotransformer based 24-pulse rectifier. *International conference on electrical and control engineering*; 2010. p. 3529–3532.

11. Singh B, Bhuvaneswari G, Garg V. A novel polygon based 18-pulse AC/DC converter for vector controlled induction motor drives. *IEEE Trans Power Electron* 2007;**22**(2):488–97.

12. Kalpana VS, Singh B. Improvement in harmonic reduction of zigzag autoconnected transformer based 12-pulse diode bridge rectifier by current injection at DC side. *IEEE Trans Indust Appl* 2017;**53**(6):5634–41.

13. Wang T, Fang F, Jiang X, Wang K, Yang L. Performance and design analysis on round-shaped transformers applied in rectifier systems. *IEEE Trans Indust Electron* 2017;**64**(2):948–55.

14. Nelson T. *787 systems and performance*. Chicago: The Boeing Company; 2005.

15. Mohan N, Robbins WP, Undeland TM, Nilssen R, Mo O. Simulation of power electronic and motion control systems-an overview. *Proc IEEE* 1994;**82**(8):1287–302.

16. Bozhko S, Wu T, Hill C, Asher G. Accelerated simulation of complex aircraft electrical power system under normal and faulty operational scenarios. *36th annual conference on IEEE industrial electronics society*; 2010 Nov 7–10; Glendale. Piscataway:IEEE Press; 2010. p. 333–8.

17. Krause PC, Asipo TA. Analysis and simplified representations of rectifier – inverter reluctance-synchronous motor drives. *IEEE Trans Power Appar Syst* 1969; PAS-88(6): 962–70.

18. Ong CM. *Dynamic simulation of electric machinery using Matlab/Simulink*. Dover: Prentic-Hall; 1997.

19. Paice DA. *Power electronic converter harmonics: multipulse methods for clean power*. Hoboken: Wiley-IEEE Press; 1996.

20. Yang T, Bozhko S, Asher G. Functional modeling of symmetrical multipulse autotransformer rectifier units for aerospace applications. *IEEE Trans Power Electron* 2015;**30**(9):4704–25.

21. Uan-Zo-li A, Burgos R, Lacaux F, Roshan A, Wang F, Boroyevich D. Analysis of new step-up and step-down direct symmetric 18-pulse topologies for aircraft autotransformer-rectifier units.*IEEE 36th power electronics specialists conference*; 2005 June 16; Recife.Piscataway:IEEE Press; 2005. p. 1142–8.

22. Wu T, Bozhko S, Asher G, Thomas D. Accelerated functional modeling of aircraft electrical power systems including fault scenarios. *35th annual conference of IEEE industrial electronics*; 2009 Nov 3–5; Porto.Piscataway:IEEE Press; 2009. p. 2537–44.